

Tracking-Assisted Object Detection with Event Cameras

Ting-Kang Yen¹, Igor Morawski¹, Shusil Dangi³, Kai He³, Chung-Yi Lin¹,
Jia-Fong Yeh¹, Hung-Ting Su¹, and Winston Hsu^{1,2}

¹ National Taiwan University

² Mobile Drive Technology

³ Qualcomm Inc.

Abstract. Event-based object detection has recently garnered attention in the computer vision community due to the exceptional properties of event cameras, such as high dynamic range and no motion blur. However, feature asynchronism and sparsity cause *invisible objects* due to no relative motion to the camera⁴, posing a significant challenge in the task. Prior works have studied various memory mechanisms to preserve as many features as possible at the current time, guided by temporal clues. While these implicit-learned memories retain some short-term information, they still struggle to preserve long-term features effectively. In this paper, we consider those invisible objects as *pseudo-occluded objects* and aim to reveal their features. Firstly, we introduce *visibility* attribute of objects and contribute an auto-labeling algorithm to append additional *visibility* labels on an existing event camera dataset. Secondly, we exploit tracking strategies for pseudo-occluded objects to maintain their permanence and retain their bounding boxes, even when features have not been available for a very long time. These strategies can be treated as an explicit-learned memory guided by the tracking objective to record the displacements of objects across frames. Lastly, we propose a spatio-temporal feature aggregation module to enrich the latent features and a consistency loss to increase the robustness of the overall pipeline. We conduct comprehensive experiments to verify our method’s effectiveness where still objects are retained but real occluded objects are discarded. The results demonstrate that (1) the additional *visibility* labels can assist in supervised training, and (2) our method outperforms state-of-the-art approaches with a significant improvement of 7.9% absolute mAP.

Keywords: Object Permanence · Spatio-Temporal Feature Aggregation
· Joint Object Detection and Tracking · Consistency Loss

1 Introduction

Event cameras measure only per-pixel intensity changes asynchronously and are suitable for detecting fast-moving objects. For those slow-moving objects or still

⁴ The objects with no relative motion to the camera, still objects, invisible objects, and pseudo-occluded objects are used interchangeably in the paper.

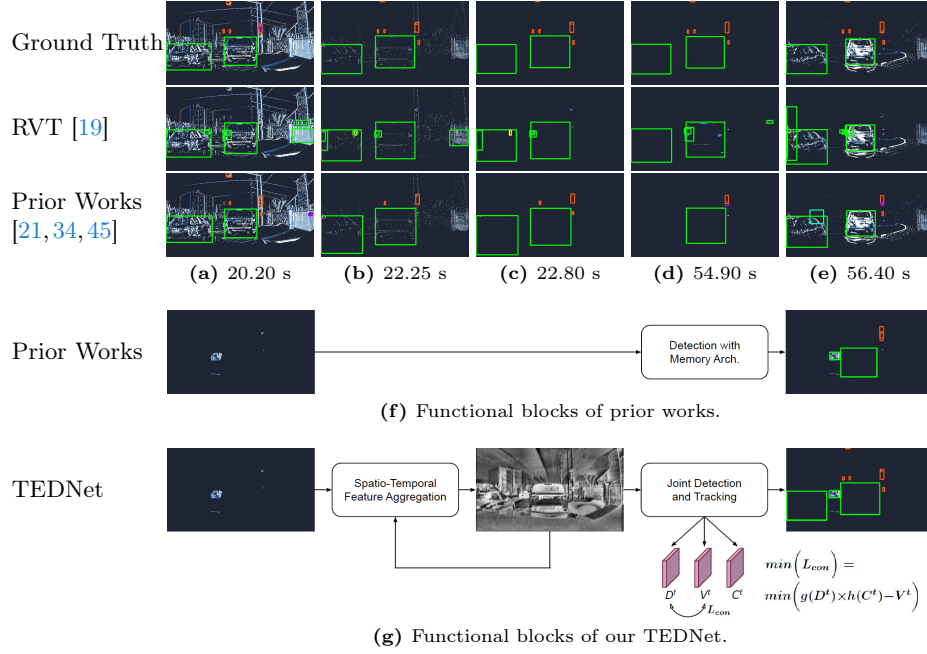


Fig. 1: A video sequence from the 1 Megapixel Automotive Detection Dataset with absolute timestamps, ground truth labels, and some detection results from prior works. Both cars slow down from 1a to 1b, remain still from 1c to 1d and start moving at 1e. Meanwhile, 1f and 1g show the main difference between prior works and our TEDNet. Bounding boxes with different colors correspond to different categories.

objects, it is very hard to notice their physical existence if there are no temporal clues. For example, Fig. 1 shows a video sequence from 1 Megapixel Automotive Detection Dataset where two cars slow down from Fig. 1a to Fig. 1b, remain still from Fig. 1c to Fig. 1d, and start moving at Fig. 1e. The features in the ground truth bounding boxes disappear gradually when slowing down, become empty when being still, and reappear gradually when speeding up. Human beings are capable of knowing the physical existence of these two cars as long as they observe the whole video sequence, even if there are no features in the ground truth bounding boxes. This kind of ability is known as object permanence [2, 3, 10]. In fact, object permanence is a term from developmental psychology that describes how infants know the continuous existence of unseen objects.

Prior works propose different kinds of memory architectures to retain object permanence in event-based object detection. RED [34] and RVT [19] propose multi-stage convolution and recurrent vision transformer with different spatial resolutions, respectively, along with multi-stage ConvLSTMs. ASTM-Net [26] proposes a temporal attention convolutional network (TACN) along with a single-stage ConvLSTM. DManet [45] and HMNet [21] propose memories with different temporal resolutions to handle objects with different speeds,

respectively. One common characteristic among these models is that they all use implicit memories with different spatial or temporal resolutions. After some experiments⁵ shown in Fig. 1, we found that only RVT [19] can better handle the long-range dependency problem, i.e. when objects slow down and there are eventually no relative motions between objects and the camera, these objects become invisible regardless of their physical existence. Meanwhile, RVT [19] produces many false positives with high confidence scores due to its implicit ConvLSTMs. Other models in Fig. 1 are memoryless as long as the duration of missing features is too long, which is over 30 seconds from Fig. 1c to Fig. 1d and degrades the mAP performance of object detection.

In this work, we propose to formulate the long-range dependency problem for still objects in event cameras as an occlusion problem and use tracking through occlusion [20, 23, 32, 42, 43] to keep the object permanence. Intuitively, some analogies exist between the long-range dependency problem for still objects and the tracking through occlusion. First, there are no features of the objects we want to detect in both cases. Second, tracking through occlusion is based on a constant velocity assumption; instead, the long-range dependency problem for still objects is based on a zero velocity assumption. Hence, tracking through occlusion can potentially solve the long-range dependency problem for still objects in event cameras. To our knowledge, we are the first to regard the long-range dependency problem in event cameras as a tracking-through-occlusion paradigm.

In order to supervise the training of object permanence, we need additional *visibility* labels to distinguish between moving objects and still objects. Hence, we propose an algorithm to perform the annotation automatically. Furthermore, our model is based on some joint object detection and tracking models, which give object detectors tracking ability. We augment these models with a spatio-temporal feature aggregation module and a consistency loss to not only enrich the latent features as shown in Fig. 1g but also increase the robustness of the overall pipeline where still objects are retained but real occluded objects are discarded. In summary, our model outperforms state-of-the-art event-based object detectors by 7.9% absolute mAP and our main contributions to this work are as follows:

1. We propose to make invisible objects visible by considering those invisible objects as pseudo-occlusion and exploiting tracking as an explicit memory to retain their bounding boxes despite having no feature for a very long time.
2. We propose an auto-labeling algorithm to annotate still objects, which are used to supervise the training of object permanence.
3. We propose a spatio-temporal feature aggregation module and a consistency loss to track still or pseudo-occluded objects instead of real occluded objects and further improve the mAP performance.

⁵ We cannot experiment on ASTMNet [26] due to no available source code. HMNet [21] is trained on GEN1 Automotive Detection Dataset with a smaller spatial resolution (304 x 240). Therefore, we downsample the spatial resolution of 1 Megapixel Automotive Detection Dataset (1280 x 720) and test them on HMNet [21] directly.

4. The efficacy of the proposed architecture has been experimented on 1 Megapixel Automotive Detection Dataset. It significantly surpasses state-of-the-art event-based object detectors by 7.9% absolute mAP.

2 Related Works

2.1 Event Representations

Event representations can be divided into sparse and dense representations according to the downstream tasks. For classification tasks, sparse or point-cloud-like representations are more commonly used; instead, for localization tasks, dense or image-like representations are more widely used except for a small portion of works that apply graphs [38] or spikes [13, 40] as an event representation for object detection.

Dense representations can be further divided into handcrafted methods and learning-based methods. There are four mainstream handcrafted methods, including *Event Histogram* [30], *Timestamp* [1, 14, 31, 33], *Time Surface* [12, 24, 39], and *Event Volume* [22, 36, 52, 53]. RED [34] has validated that *Event Volume* gets better mAP performance in event-based object detection compared with other handcrafted event representations.

For learning-based methods, EST [18] and Matrix-LSTM [11] are designed for classification tasks instead of localization tasks. In addition, ASTMNet [26], DMANet [45], and HMNet [26] propose different learning-based event representations for object detection and get some mAP performance improvements.

2.2 Object Detection with Event Cameras

Object detection with event cameras can be categorized into three branches according to the event representations and network architectures, including GNN-based, SNN-based, and DNN-based methods. GNN-based [38] and SNN-based [13, 40] methods are more challenging due to inferior message propagation through a graph and difficulties in optimization, respectively. DNN-based methods [19, 21, 26, 34, 45] convert sparse events in a time window to a dense event representation that discards some temporal information due to sampling and apply deep neural networks for object detection. Hence, how to obtain better spatio-temporal features across adjacent frames becomes crucial to enhance the performance of event-based object detection, which is very similar to video object detection tasks [16, 27, 41, 47]. Different kinds of memory architectures are proposed to retain better spatio-temporal features, including multi-stage ConvLSTMs in RED [34] and RVT [19], TACN and a single-stage ConvLSTM in ASTMNet [26], long and short memories in DMANet [45], and an attention-based hierarchical memory in HMNet [21]. Although these memory architectures can memorize historical information for a while, most of them are still forgettable after a very long time and degrade the mAP performance of object detections.

2.3 Multi-Object Tracking

Multi-object tracking can be divided into two branches, including *tracking by detection* and *joint object detection and tracking*, where object detection and bounding box association are performed separately and jointly, respectively. The most challenging problem in multi-object tracking is *tracking with long-term occlusions* where tracking identity needs to be maintained even though occlusion incurs temporal invisibility.

Tracking by Detection is a two-stage method where object detection and bounding box association are performed separately. It can be further categorized into online [7, 9, 46, 48] and offline [4, 5, 8, 25, 35] approaches according to whether the current bounding box association can refer to the future bounding boxes or not. In this work, we focus on online approaches because they are causal and more practical in real scenarios. SORT [7] and DeepSORT [46] are two classical works to apply the Kalman filter for bounding box association. The only difference between these two works is that the bounding box association policy in SORT [7] is based on the intersection over union (IOU) of two bounding boxes, and the association policy in DeepSORT [46] is based on the appearance features from a deep neural network, which makes it more robust to deal with occlusion in longer periods of time. These rule-based approaches lack generalizability and make them harder to transfer to different scenarios.

Joint Object Detection and Tracking is a one-stage and online method where object detection and bounding box association are performed jointly by an end-to-end trainable deep neural network. [6] converts Faster R-CNN [37] to a *Tracktor* by utilizing bounding box regression to predict the bounding boxes of the next frame. CenterTrack [50] is built on top of CenterNet [15, 51] and outputs not only bounding box locations but also tracking vectors, i.e., a vector from the bounding box center of the current frame to the corresponding bounding box center of the previous frame. PermaTrack [43] is built on top of CenterTrack [50] and is able to track invisible objects for a long-term feature disappearance by supervising the visibility property during the training stage. RetinaTrack [28] is built on top of RetinaNet [29] and is able to track occluded objects by using instance-level features to perform bounding box association. These learning-based approaches can better keep the object permanence in the presence of long-term occlusions.

3 Method

Our Tracking-assisted Event-based object Detector is denoted TEDNet which consists of four modules, including *event-to-tensor conversion*, *spatio-temporal feature aggregation*, *joint object detection and tracking*, and *consistency loss* as shown in Fig. 2. First, input events are sampled with a constant time window and converted to a dense event representation. Then, the dense tensor is passed

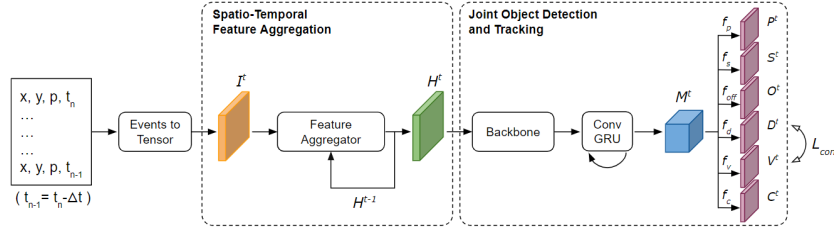


Fig. 2: The architecture of the proposed TEDNet.

through a *spatio-temporal feature aggregator* to retain as much spatio-temporal information as possible, especially for those still objects with no features. After that, a *joint object detection and tracking* module is used to track those still objects according to the object permanence property. Finally, a *consistency loss* correlates two feature maps and increases the robustness of the overall pipeline. In addition, an auto-labeling algorithm is proposed to supervise the training of object permanence by distinguishing between moving objects and still objects. All of the details are elaborated in the latter parts of this section.

3.1 Auto-Labeling for Still Objects

The labels for object detection in 1 Megapixel Automotive Detection Dataset come from the inference results of its corresponding RGB images. It offers only bounding boxes and tracking identities, which are insufficient for an object detector to keep object permanence for still objects. Therefore, we propose an algorithm to split objects into still objects and moving objects automatically to supervise the training of object permanence, as shown in Algorithm 1. In a nutshell, still objects are invisible by an event camera where *visibility* labels are annotated as 0.0. However, moving objects are visible by an event camera where *visibility* labels are annotated as 1.0. The criteria to decide whether an object is still are based on the feature sparsity in the bounding box and the displacement between centers of two bounding boxes with the same tracking identity in adjacent frames. In the following, the overall procedures are divided into three parts, including *calculation of occupancy rate*, *calculation of displacement*, and *continuity maintenance*.

Calculation of Occupancy Rate is to determine whether the features of an object are sparse or not. First, input features of shape $[C, H, W]$ for i -th frame are converted to a binary mask dubbed *occupancy_mask* in Line 6 of Algorithm 1. The *occupancy_mask* is a tensor of shape $[H, W]$ indicating whether at least one event appears at a specific pixel location in the time duration $[(i-1) \times \Delta t, i \times \Delta t)$ or not, where $i \in [1, T]$ is the frame identity and Δt is the constant time window. Then, *occ_mask* is obtained by slicing the corresponding bounding box region in Line 8. Next, *bbox_mask* is obtained by

discarding the overlapping regions with other bounding boxes in Line 9. In more detail, $bbox_mask$ is a tensor of shape $[h_j, w_j]$, which is the same as occ_mask , where all pixel values are initialized to 1 and pixel values in those locations that overlap with other bounding boxes are turned to 0. After that, occ_true is calculated by Eq. (1) representing the number of most possible occupied pixels for the corresponding object, and occ_false is calculated by Eq. (2) representing the number of most certain pixels for the background. Finally, occ_rate is obtained by Eq. (3) in Line 10, which is a ratio indicating how much percentage of pixel values of 1 in $bbox_mask$ are occupied by occ_mask . In summary, the occupancy rate represents the feature sparsity of a specific object. Its value is high in moving objects due to more features and is low in still objects due to fewer or no features.

$$occ_true = \sum_{\substack{0 < x < w_j \\ 0 < y < h_j}} (occ_mask(x, y) == 1) \times bbox_mask(x, y) \quad (1)$$

$$occ_false = \sum_{\substack{0 < x < w_j \\ 0 < y < h_j}} (occ_mask(x, y) == 0) \times bbox_mask(x, y) \quad (2)$$

$$occ_rate = \frac{occ_true}{occ_true + occ_false} \quad (3)$$

Calculation of Displacement is to approximate the motion property of the corresponding object by the bounding box center in the current frame $[c_x, c_y]$ and that with the same tracking identity in the previous frame $[pc_x, pc_y]$ from Line 13 to 16. The displacement is normalized by the width and height of the current bounding box by Eq. (4) in Line 16 to discard the drifting effect of inaccurate bounding boxes for both small and large still objects. As a matter of fact, this approximation is inaccurate due to the lack of depth information in event cameras. Therefore, the decision-making of still objects depends on not only displacement but also occupancy rate.

$$disp = \sqrt{\left(\frac{pc_x - c_x}{w_j}\right)^2 + \left(\frac{pc_y - c_y}{h_j}\right)^2} \quad (4)$$

Continuity Maintenance is used to make the variation of *visibility* label for each specific tracking identity as smooth as possible and discard those bounding boxes with no features at their first occurrence. If there is no corresponding bounding box with the same tracking identity in the previous frame, a *visibility* label is determined by only the occupancy rate from Line 24 to 26. Also, a buffer dubbed *still_hits* is needed to memorize the number of still hits for each tracking identity individually in the history and smooth out the impulse of *visibility* variation owing to the original label noises. If there is a corresponding

tracked object in the previous frame, a *visibility* label is determined by either both occupancy rate and displacement from Line 17 to 19 or only the *still_hits* buffer from Line 20 to 22. Finally, not only visible objects but also those invisible objects that are tracked for two previous frames are added to the new labels from Line 28 to 30. As a result, only N_i out of M_i objects are preserved with additional *visibility* labels for i -th frame.

3.2 Event Representation

Prior works have proved that learning-based event representations [21, 26, 45] outperform handcrafted event representations [19, 34], but learning-based methods have higher computational complexity, which makes training slow. In this work, we do not focus on designing new event representations; instead, we opt for the best-performing handcrafted event representation [34], i.e., *Event Volume*, as our *event-to-tensor conversion* module. The benefit of using handcrafted methods is that they can be preprocessed in advance instead of on-the-fly processing like learning-based methods. As a result, we can focus on retaining object permanence to enhance object detection performance with faster training speed.

3.3 Spatio-Temporal Feature Aggregation

The most significant challenge in event cameras is the long-range dependency problem. In this work, we propose to apply either a simple 3D convolutional network(*C3D*) [44] or a deformable 3D convolutional network(*D3D*) [49] as well as a ConvGRU in *joint object detection and tracking* module as our spatio-temporal feature aggregator. Unlike [44, 49] that input a video sequence to get a better spatio-temporal feature for the downstream task, our approach inputs only two frames, i.e., a current frame I_t and a previous history frame H_{t-1} . The current history frame is obtained by $H_t = X3D(I_t, H_{t-1})$ where *X3D* is either *C3D* or *D3D*. To be more specific, we integrate a 3D convolution with a recurrent neural network to get a better spatio-temporal feature as an input to the following *joint object detection and tracking* module.

While both 3D convolution and ConvGRU are effective for aggregating spatio-temporal features, 3D convolution tends to be more computationally efficient, especially when the input feature has high spatial resolution. Therefore, we opt for 3D convolution on the input side where I_t and H_t have the same spatial resolution and ConvGRU on the output side where M_t is downsampled by 4 times from I_t as shown in Fig. 2.

3.4 Joint Object Detection and Tracking

Although *tracking by detection* is a classical tracking paradigm, it has some intrinsic drawbacks due to its two-stage properties where bounding box association fails if occlusion causes incorrect detection. Hence, in this work, we propose to apply a one-stage *joint object detection and tracking* method to better leverage

Algorithm 1: Auto-labeling for still objects

Input: $inputFeatures$ = tensor of shape $[T, C, H, W]$
 $oldLabels[i] = \{[x_j, y_j, w_j, h_j, trackId_j] \mid j \in [1, M_i]\},$
 $i \in [1, T]$

Output:
 $newLabels[i] = \{[x_k, y_k, w_k, h_k, trackId_k, visibility_k] \mid$
 $k \in [1, N_i]\}, i \in [1, T]$

```

1  $\Delta t \leftarrow 50000 \mu s;$ 
2  $still\_hits \leftarrow \{\};$ 
   /* key-value pairs where values are limited to 5. */
3  $track\_vis \leftarrow \{\};$ 
   /* key-value pairs where values are queues with size 2. */
4 for  $i \leftarrow 1$  to  $T$  do
5    $newLabels[i] \leftarrow \{\};$ 
6    $occupancy\_mask = get\_occupancy\_mask(inputFeatures[i]);$ 
7   foreach  $[x_j, y_j, w_j, h_j, trackId_j] \in oldLabels[i]$  do
8      $occ\_mask = occupancy\_mask[x_j : x_j + w_j, y_j : y_j + h_j];$ 
9      $bbox\_mask = get\_bbox\_mask(x_j, y_j, w_j, h_j, oldLabels[i]);$ 
10     $occ\_rate = get\_occupancy\_rate(occ\_mask, bbox\_mask);$ 
11     $visibility_j \leftarrow 1.0;$  /* Initialize to a moving object. */
12    if  $trackId_j$  in  $newLabels[i-1]$  then
13       $c_x, c_y = get\_bbox\_center(x_j, y_j, w_j, h_j);$ 
14       $x_k, y_k, w_k, h_k, trackId_k, visibility_k =$ 
         $get\_previous\_bbox(trackId_j, newLabels[i-1]);$ 
15       $pc_x, pc_y = get\_bbox\_center(x_k, y_k, w_k, h_k);$ 
16       $disp = get\_normalized\_displacement(pc_x, pc_y, c_x, c_y);$ 
17      if  $disp < D_{value}$  and  $occ\_rate < O_{value}$  then
18         $visibility_j \leftarrow 0.0;$  /* Change to a still object. */
19         $still\_hits[trackId_j] \leftarrow still\_hits[trackId_j] + 1;$ 
20      else if  $still\_hits[trackId_j] > 0$  then
21         $visibility_j \leftarrow 0.0;$  /* Change to a still object. */
22         $still\_hits[trackId_j] \leftarrow still\_hits[trackId_j] - 1;$ 
23      end
24    else if  $occ\_rate < O_{value}$  then
25       $visibility_j \leftarrow 0.0;$  /* Change to a still object. */
26       $still\_hits[trackId_j] \leftarrow still\_hits[trackId_j] + 1;$ 
27    end
28    if  $visibility_j = 1.0$  or  $(track\_vis[trackId_j][0] = i - 2$  and
       $track\_vis[trackId_j][1] = i - 1)$  then
29       $newLabels[i].add([x_j, y_j, w_j, h_j, trackId_j, visibility_j]);$ 
30       $track\_vis[trackId_j].enqueue(i);$ 
31    end
32  end
33 end

```

tracking capability to enhance object detection performance. Two candidates for the *joint object detection and tracking* method are CenterTrack [50] and PermaTrack [43]. In addition to the localization head f_p , size head f_s , and offset head f_{off} in CenterNet [15, 51], CenterTrack [50] adds one extra displacement head f_d for tracking, which represents a tracking vector from the bounding box center of the current frame to the corresponding bounding box center of the previous frame. PermaTrack [43] adds one more visibility head f_v to represent the occlusion ratio, i.e., if an object is not occluded, fully occluded, or partially occluded, its visibility is 1.0, 0.0, or between 0.0 and 1.0, respectively. In the situation of event cameras, visibility head f_v is used to represent the mobility ratio, i.e., if an object is still or moving, its visibility is 0.0 or 1.0, respectively. There is no visibility value between 0.0 and 1.0 because it is hard to determine the accurate velocity by using only 2D image coordinates as mentioned in Sec. 3.1.

3.5 Consistency Loss

The displacement head f_d outputs a displacement map $D^t \in \mathbb{R}^{\frac{H}{R} \times \frac{W}{R} \times 2}$ to represent the tracking vectors of every object with downsampling factor $R = 4$. However, the visibility head f_v outputs a visibility map $V^t \in [0, 1]^{\frac{H}{R} \times \frac{W}{R}}$ to represent whether the center coordinates p_i^t of i -th detected object is still or not. Both D^t and V^t imply the mobility of objects in two different forms with different channels and magnitudes. To be more concrete, D^t and V^t have some proportional relationship after some transformation, i.e. $V^t \propto g(D^t)$ where $g(D^t) = \|D^t\|_2 \in \mathbb{R}^{\frac{H}{R} \times \frac{W}{R}}$ is an Euclidean norm of D^t representing the magnitude of movements. In this work, we propose another consistency head f_c that outputs a consistency map C^t to model the proportional relationship where the learnable proportional ratio is $h(C^t) = e^{-relu(C^t)} \in [0, 1]^{\frac{H}{R} \times \frac{W}{R}}$ and our learning goal is to minimize the difference between $g(D^t) \times h(C^t)$ and V^t , i.e. consistency loss, by regression as shown in Eq. (5). As a result, the consistency loss between D^t and V^t is shown in Eq. (6) where p_i belongs to visible objects.

$$\min(L_{con}) = \min\left(\left|g(D^t) \times h(C^t) - V^t\right|\right) = \min\left(\left|\|D^t\|_2 \times e^{-relu(C^t)} - V^t\right|\right) \quad (5)$$

$$L_{con} = \frac{1}{N} \sum_{i=1}^N \left| \|D_{p_i}^t\|_2 \times e^{-relu(C_{p_i}^t)} - V_{p_i}^t \right| \quad (6)$$

4 Experiments

4.1 Dataset with Auto-Labeling

Prophesee, a company developing event-based sensors and algorithms, released the first large-scale and high-resolution (1280×720) event-based object detection dataset and its deep neural network RED [34] for automotive scenarios. This

Table 1: The effectiveness of the auto-labeling algorithm by RED [34]

mAP@0.5		Train on	
		noisy GT	clean GT
Test on	noisy GT	43.5	43.6
	clean GT	47.1	48.2

1 Megapixel Automotive Detection Dataset is captured by the 1-megapixel event camera [17] and a standard RGB camera, but only event data and its annotations are released. The annotations come from the inference result of the RGB image and transfer to the event camera coordinate by geometric transformation. After visualizing the annotations in the dataset, we found that there are several incorrect bounding boxes with either imprecise locations and sizes or incorrect labels. Most importantly, several bounding boxes contain no features at the very beginning of some videos because they are still and visible by an RGB camera but invisible by an event camera, and humans cannot recognize their physical existence with only event data even though we have temporal clues. These incorrect bounding boxes limit the object detection performance and make model training awkward. Therefore, we clean the dataset by an auto-labeling algorithm in Sec. 3.1 with hyperparameters $D_{value}=0.03$ and $O_{value}=0.1$ to not only insert additional *visibility* labels to supervise the training of object permanence but also discard those bounding boxes that are impossible to be detected by humans. We named the dataset before/after data cleaning *noisy GT/clean GT* and its corresponding model *noisy model/clean model*.

To validate the effectiveness of the proposed auto-labeling algorithm, we train and test the RED [34] on both *noisy GT* and *clean GT* by using the training and testing set respectively, and evaluate the performance by using mAP@0.5 as shown in Tab. 1. The first row shows that data cleaning does not degrade the model performances on *noisy GT*. The first or second column shows that mAP increases on *clean GT* because those impossible-to-detect objects are discarded successfully. The second row shows that mAP increases with *clean model* because the auto-labeling algorithm effectively makes model training more robust.

4.2 Ablation Study

The models in ablation studies are trained on *clean GT* and tested on both *noisy GT* and *clean GT* as shown in Tab. 2. We choose two *joint object detection and tracking* models as our baselines, CenterTrack and PermaTrack [43], respectively. The CenterTrack shown here is the original one [50] with ConvGRU, making it comparable with PermaTrack [43].

Spatio-Temporal Feature Aggregation We study two *spatio-temporal feature aggregation* approaches along with CenterTrack [50] and PermaTrack [43].

Table 2: Ablation study of each component in our TEDNet

Methods	(a)	(b)	(c)	(d)	(e)	(f)	(g)	(h)	TEDNet
CenterTrack*	✓	✓	✓						
PermaTrack				✓	✓	✓	✓	✓	✓
D3D		✓			✓				✓
C3D			✓			✓		✓	
L_{con}							✓	✓	✓
mAP@0.5									
noisy GT	48.3	53.9	53.4	48.8	53.8	55.0	51.1	54.1	56.2
clean GT	54.1	59.7	59.2	55.2	60.5	61.2	57.7	60.8	62.8

* The CenterTrack here is the original one with ConvGRU.

Comparing (b) with (c), *D3D* performs slightly better than *C3D* if we use CenterTrack [50] as the baseline. However, comparing (e) with (f), we are surprised that *C3D* is slightly superior to *D3D* if we use PermaTrack [43] as the baseline. Intuitively, *C3D* is the performance lower bound of *D3D* with the same convolution kernel size (3×3), but *D3D* introduces additional parameters to learn offsets, making it harder to converge. Therefore, we need more fine-grained hyperparameter tuning or regularization to harness the advantages of deformable convolutions. In summary, *spatio-temporal feature aggregation* improves the mAP@0.5 by 5.0% to 6.2% compared with the corresponding baselines.

Consistency Loss We conduct consistency loss between displacement map D^t and visibility map V^t to model their proportional relationship. Consistency loss can only be applied to PermaTrack [43] because there is no visibility head in CenterTrack [50]. Comparing (d) with (g), the consistency loss enhances the mAP@0.5 by 2.3% on *noisy GT* and 2.5% on *clean GT*. Comparing (f) with (h), the consistency loss degrades the mAP@0.5 by 0.9% on *noisy GT* and 0.4% on *clean GT* if we use *C3D* as the *spatio-temporal feature aggregation* module. In contrast, comparing (e) with our TEDNet, the consistency loss improves the mAP@0.5 by 2.4% on *noisy GT* and 2.3% on *clean GT* if we use *D3D* as the *spatio-temporal feature aggregation* module. To sum up, consistency loss offers a better regularization to harness the advantages of deformable convolutions and increases the robustness of the overall pipeline.

4.3 Comparison with the State-of-the-art

We compare our TEDNet to the state-of-the-art event-based object detectors on both *noisy GT* in Tab. 3 and *clean GT* in Tab. 4. Our method outperforms the state-of-the-art model by 7.9% absolute mAP@0.5 and achieves 56.2% on *noisy GT* as shown in Tab. 3. In addition, our method outperforms RED [34], CenterTrack [50], and PermaTrack [43] by 14.6%, 8.7%, and 7.6% absolute mAP@0.5 respectively and achieves 62.8% on *clean GT* as shown in Tab. 4.

Table 3: Performance comparison with the state-of-the-art event-based object detectors on **noisy GT**. Runtime is measured by GeForce RTX 3090 GPU where ASTMNet [26] does not offer source code, but it should be 5.5 times slower than RVT [19] and 1.8 times slower than RED [34] according to [19].

Methods	mAP@0.5	mAP	params(M)	GFLOPs	runtime(ms)
RED [34]	43.5	22.5	24.1	31.2	11.5
ASTMNet [26]	48.3	-	>100 [19]	-	>20.0
RVT [19]	47.0	-	18.5	15.2	5.6
DMANet [45]	46.3	24.7	28.2	62.2	15.1
CenterTrack [50] ^{*†}	48.3	25.3	21.0	46.5	12.2
PermaTrack [43] [†]	48.8	26.0	21.2	46.5	12.4
TEDNet(Ours)[†]	56.2	31.2	21.3	48.8	13.5

^{*} The CenterTrack here is the original one with ConvGRU.

[†] These models are trained on clean GT but tested on noisy GT.

Other models are trained and tested on noisy GT.

Table 4: Performance comparison with the state-of-the-art event-based object detectors on **clean GT**.

Methods	mAP@0.5	mAP
RED [34]	48.2	25.9
CenterTrack [50]	54.1	29.3
PermaTrack [43]	55.2	30.2
TEDNet(Ours)	62.8	35.8

4.4 Visualization of Detection Results

We visualize the detection results in Fig. 3 by a video with two cars remaining still for over 30 seconds and some other cars passing in front of them in between. For RED [34], RVT [19], DMANet [45], and HMNet [21], visualizations are built on top of their visualized image converted from event data directly by Metavision SDK of Prophesee because their latent feature maps contain much larger channels and smaller spatial resolutions, making them hard to visualize. For our TEDNet, visualizations are built on top of their latent feature maps H^t , which contain fewer channels and the same spatial resolutions as their input feature maps I^t . While the values scatter everywhere in latent feature maps H^t due to $D3D$ and hence visualization is difficult, we apply an adaptive histogram equalization method called CLAHE [54] to each channel in H^t individually to enhance the contrast and choose one with the best appearance. For CenterTrack [50] and PermaTrack [43], visualizations are built on top of their input feature maps I^t , and CLAHE [54] is also applied to each channel in which one with the best appearance is chosen to be comparable with TEDNet.

Either one or two false negatives occur in the duration between 3rd and 4th frames of RED [34], DMANet [45], and HMNet [21]. To be more specific, the

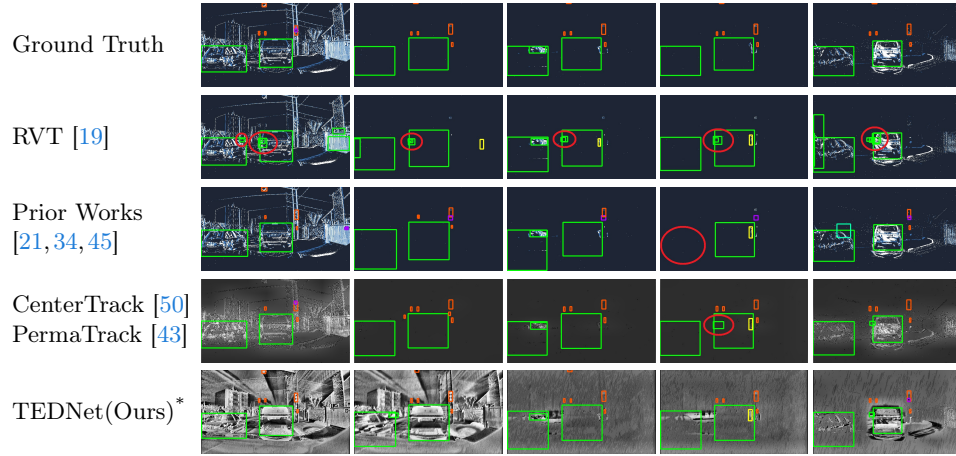


Fig. 3: The visualization results of prior works [19, 21, 34, 43, 45, 50] and our TEDNet. Bounding boxes with different colors correspond to different categories. Red circles correspond to either false positives or false negatives. TEDNet achieves state-of-the-art mAP performance by retaining bounding boxes of still objects and discarding bounding boxes of real occluded objects. (Note: * shows the post-processed feature map after the spatio-temporal feature aggregation.)

false negatives last 17.9 seconds in RED [34], 32.4 seconds in DMANet [45], and interweavingly in HMNet [21], representing the severity of the long-range dependency problem. CenterTrack [50] and PermaTrack [43] solve the false negatives by tracking still objects. However, they incur additional false positives shown in the 4th frame of CenterTrack [50] and PermaTrack [43]. These false positives occur when a moving car passes in front of a still car from the 3rd frame and becomes fully occluded in the 4th frame where the tracking module regards that object as a still object and keeps tracking it. To be more concrete, CenterTrack [50] and PermaTrack [43] are unable to distinguish between still and real occluded objects and hence produce many false positives. In contrast, our TEDNet can retain only still objects and discard real occluded objects because $D3D$ and *consistency loss* retain the clearest spatial-temporal information among all other models and make invisible objects visible.

5 Conclusion

We introduce a novel architecture to apply tracking through occlusion to solve the long-range dependency problem for still objects in event cameras. The architecture retains the most abundant spatial-temporal information and tracks only still or pseudo-occluded objects instead of real occluded objects. Our comprehensive experiments demonstrate the effectiveness of each component of our

TEDNet that achieves state-of-the-art performance in event-based object detection. In addition, we propose an auto-labeling algorithm to not only add additional labels for still objects to supervise the training of object permanence but also discard those impossible-to-detect objects at the very beginning of some videos to make model training more robust.

References

1. Bai, W., Chen, Y., Feng, R., Zheng, Y.: Accurate and efficient frame-based event representation for aer object recognition. In: 2022 International Joint Conference on Neural Networks (IJCNN). pp. 1–6. IEEE (2022) 4
2. Baillargeon, R., DeVos, J.: Object permanence in young infants: Further evidence. *Child development* **62**(6), 1227–1246 (1991) 2
3. Baillargeon, R., Spelke, E.S., Wasserman, S.: Object permanence in five-month-old infants. *Cognition* **20**(3), 191–208 (1985) 2
4. Berclaz, J., Fleuret, F., Fua, P.: Robust people tracking with global trajectory optimization. In: 2006 IEEE Computer Society Conference on Computer Vision and Pattern Recognition (CVPR’06). vol. 1, pp. 744–750. IEEE (2006) 5
5. Berclaz, J., Fleuret, F., Turetken, E., Fua, P.: Multiple object tracking using k-shortest paths optimization. *IEEE transactions on pattern analysis and machine intelligence* **33**(9), 1806–1819 (2011) 5
6. Bergmann, P., Meinhardt, T., Leal-Taixe, L.: Tracking without bells and whistles. In: Proceedings of the IEEE/CVF International Conference on Computer Vision. pp. 941–951 (2019) 5
7. Bewley, A., Ge, Z., Ott, L., Ramos, F., Upcroft, B.: Simple online and realtime tracking. In: 2016 IEEE international conference on image processing (ICIP). pp. 3464–3468. IEEE (2016) 5
8. Brasó, G., Leal-Taixé, L.: Learning a neural solver for multiple object tracking. In: Proceedings of the IEEE/CVF conference on computer vision and pattern recognition. pp. 6247–6257 (2020) 5
9. Breitenstein, M.D., Reichlin, F., Leibe, B., Koller-Meier, E., Van Gool, L.: Robust tracking-by-detection using a detector confidence particle filter. In: 2009 IEEE 12th International Conference on Computer Vision. pp. 1515–1522. IEEE (2009) 5
10. Bremner, J.G., Slater, A.M., Johnson, S.P.: Perception of object persistence: The origins of object permanence in infancy. *Child Development Perspectives* **9**(1), 7–13 (2015) 2
11. Cannici, M., Ciccone, M., Romanoni, A., Matteucci, M.: A differentiable recurrent surface for asynchronous event-based data. In: Computer Vision–ECCV 2020: 16th European Conference, Glasgow, UK, August 23–28, 2020, Proceedings, Part XX 16. pp. 136–152. Springer (2020) 4
12. Chen, H., Suter, D., Wu, Q., Wang, H.: End-to-end learning of object motion estimation from retinal events for event-based object tracking. In: Proceedings of the AAAI Conference on Artificial Intelligence. vol. 34, pp. 10534–10541 (2020) 4
13. Cordone, L., Miramond, B., Thierion, P.: Object detection with spiking neural networks on automotive event data. In: 2022 International Joint Conference on Neural Networks (IJCNN). pp. 1–8. IEEE (2022) 4
14. Deng, Y., Li, Y., Chen, H.: Amae: Adaptive motion-agnostic encoder for event-based object classification. *IEEE Robotics and Automation Letters* **5**(3), 4596–4603 (2020) 4

15. Duan, K., Bai, S., Xie, L., Qi, H., Huang, Q., Tian, Q.: Centernet: Keypoint triplets for object detection. In: Proceedings of the IEEE/CVF international conference on computer vision. pp. 6569–6578 (2019) [5](#), [10](#)
16. Feichtenhofer, C., Fan, H., Malik, J., He, K.: Slowfast networks for video recognition. In: Proceedings of the IEEE/CVF international conference on computer vision. pp. 6202–6211 (2019) [4](#)
17. Finatou, T., Niwa, A., Matolin, D., Tsuchimoto, K., Mascheroni, A., Reynaud, E., Mostafalu, P., Brady, F., Chotard, L., LeGoff, F., et al.: 5.10 a 1280 × 720 back-illuminated stacked temporal contrast event-based vision sensor with 4.86 μm pixels, 1.066 gepps readout, programmable event-rate controller and compressive data-formatting pipeline. In: 2020 IEEE International Solid-State Circuits Conference-(ISSCC). pp. 112–114. IEEE (2020) [11](#)
18. Gehrig, D., Loquercio, A., Derpanis, K.G., Scaramuzza, D.: End-to-end learning of representations for asynchronous event-based data. In: Proceedings of the IEEE/CVF International Conference on Computer Vision. pp. 5633–5643 (2019) [4](#)
19. Gehrig, M., Scaramuzza, D.: Recurrent vision transformers for object detection with event cameras. In: Proceedings of the IEEE/CVF Conference on Computer Vision and Pattern Recognition. pp. 13884–13893 (2023) [2](#), [3](#), [4](#), [8](#), [13](#), [14](#)
20. Grabner, H., Matas, J., Van Gool, L., Cattin, P.: Tracking the invisible: Learning where the object might be. In: 2010 IEEE Computer Society Conference on Computer Vision and Pattern Recognition. pp. 1285–1292. IEEE (2010) [3](#)
21. Hamaguchi, R., Furukawa, Y., Onishi, M., Sakurada, K.: Hierarchical neural memory network for low latency event processing. In: Proceedings of the IEEE/CVF Conference on Computer Vision and Pattern Recognition. pp. 22867–22876 (2023) [2](#), [3](#), [4](#), [8](#), [13](#), [14](#)
22. Hu, Y., Delbruck, T., Liu, S.C.: Learning to exploit multiple vision modalities by using grafted networks. In: European Conference on Computer Vision. pp. 85–101. Springer (2020) [4](#)
23. Huang, Y., Essa, I.: Tracking multiple objects through occlusions. In: 2005 IEEE Computer Society Conference on Computer Vision and Pattern Recognition (CVPR’05). vol. 2, pp. 1051–1058. IEEE (2005) [3](#)
24. Lagorce, X., Orchard, G., Galluppi, F., Shi, B.E., Benosman, R.B.: Hots: a hierarchy of event-based time-surfaces for pattern recognition. IEEE transactions on pattern analysis and machine intelligence **39**(7), 1346–1359 (2016) [4](#)
25. Leal-Taixé, L., Fenzi, M., Kuznetsova, A., Rosenhahn, B., Savarese, S.: Learning an image-based motion context for multiple people tracking. In: Proceedings of the IEEE conference on computer vision and pattern recognition. pp. 3542–3549 (2014) [5](#)
26. Li, J., Li, J., Zhu, L., Xiang, X., Huang, T., Tian, Y.: Asynchronous spatio-temporal memory network for continuous event-based object detection. IEEE Transactions on Image Processing **31**, 2975–2987 (2022) [2](#), [3](#), [4](#), [8](#), [13](#)
27. Liang, Y., Wang, Z.: Video object detection based on deformable convolution. In: Proceedings of the 2020 3rd Artificial Intelligence and Cloud Computing Conference. pp. 1–4 (2020) [4](#)
28. Lu, Z., Rathod, V., Votel, R., Huang, J.: Retinatrack: Online single stage joint detection and tracking. In: Proceedings of the IEEE/CVF conference on computer vision and pattern recognition. pp. 14668–14678 (2020) [5](#)
29. Lu, Z., Rathod, V., Votel, R., Huang, J.: Retinatrack: Online single stage joint detection and tracking. In: Proceedings of the IEEE/CVF conference on computer vision and pattern recognition. pp. 14668–14678 (2020) [5](#)

30. Maqueda, A.I., Loquercio, A., Gallego, G., García, N., Scaramuzza, D.: Event-based vision meets deep learning on steering prediction for self-driving cars. In: Proceedings of the IEEE conference on computer vision and pattern recognition. pp. 5419–5427 (2018) [4](#)
31. Mitrokhin, A., Fermüller, C., Parameshwara, C., Aloimonos, Y.: Event-based moving object detection and tracking. In: 2018 IEEE/RSJ International Conference on Intelligent Robots and Systems (IROS). pp. 1–9. IEEE (2018) [4](#)
32. Papadourakis, V., Argyros, A.: Multiple objects tracking in the presence of long-term occlusions. *Computer Vision and Image Understanding* **114**(7), 835–846 (2010) [3](#)
33. Park, P.K., Cho, B.H., Park, J.M., Lee, K., Kim, H.Y., Kang, H.A., Lee, H.G., Woo, J., Roh, Y., Lee, W.J., et al.: Performance improvement of deep learning based gesture recognition using spatiotemporal demosaicing technique. In: 2016 IEEE International Conference on Image Processing (ICIP). pp. 1624–1628. IEEE (2016) [4](#)
34. Perot, E., De Tournemire, P., Nitti, D., Masci, J., Sironi, A.: Learning to detect objects with a 1 megapixel event camera. *Advances in Neural Information Processing Systems* **33**, 16639–16652 (2020) [2](#), [4](#), [8](#), [10](#), [11](#), [12](#), [13](#), [14](#)
35. Pirsiavash, H., Ramanan, D., Fowlkes, C.C.: Globally-optimal greedy algorithms for tracking a variable number of objects. In: CVPR 2011. pp. 1201–1208. IEEE (2011) [5](#)
36. Rebecq, H., Ranftl, R., Koltun, V., Scaramuzza, D.: Events-to-video: Bringing modern computer vision to event cameras. In: Proceedings of the IEEE/CVF Conference on Computer Vision and Pattern Recognition. pp. 3857–3866 (2019) [4](#)
37. Ren, S., He, K., Girshick, R., Sun, J.: Faster r-cnn: Towards real-time object detection with region proposal networks. *Advances in neural information processing systems* **28** (2015) [5](#)
38. Schaefer, S., Gehrig, D., Scaramuzza, D.: Aegnn: Asynchronous event-based graph neural networks. In: Proceedings of the IEEE/CVF conference on computer vision and pattern recognition. pp. 12371–12381 (2022) [4](#)
39. Sironi, A., Brambilla, M., Bourdis, N., Lagorce, X., Benosman, R.: Hats: Histograms of averaged time surfaces for robust event-based object classification. In: Proceedings of the IEEE conference on computer vision and pattern recognition. pp. 1731–1740 (2018) [4](#)
40. Su, Q., Chou, Y., Hu, Y., Li, J., Mei, S., Zhang, Z., Li, G.: Deep directly-trained spiking neural networks for object detection. In: Proceedings of the IEEE/CVF International Conference on Computer Vision. pp. 6555–6565 (2023) [4](#)
41. Sun, G., Hua, Y., Hu, G., Robertson, N.: Efficient one-stage video object detection by exploiting temporal consistency. In: European Conference on Computer Vision. pp. 1–16. Springer (2022) [4](#)
42. Tokmakov, P., Jabri, A., Li, J., Gaidon, A.: Object permanence emerges in a random walk along memory. *arXiv preprint arXiv:2204.01784* (2022) [3](#)
43. Tokmakov, P., Li, J., Burgard, W., Gaidon, A.: Learning to track with object permanence. In: Proceedings of the IEEE/CVF International Conference on Computer Vision. pp. 10860–10869 (2021) [3](#), [5](#), [10](#), [11](#), [12](#), [13](#), [14](#)
44. Tran, D., Bourdev, L., Fergus, R., Torresani, L., Paluri, M.: Learning spatiotemporal features with 3d convolutional networks. In: Proceedings of the IEEE international conference on computer vision. pp. 4489–4497 (2015) [8](#)
45. Wang, D., Jia, X., Zhang, Y., Zhang, X., Wang, Y., Zhang, Z., Wang, D., Lu, H.: Dual memory aggregation network for event-based object detection with learnable

- representation. In: Proceedings of the AAAI Conference on Artificial Intelligence (2023) [2](#), [4](#), [8](#), [13](#), [14](#)
46. Wojke, N., Bewley, A., Paulus, D.: Simple online and realtime tracking with a deep association metric. In: 2017 IEEE international conference on image processing (ICIP). pp. 3645–3649. IEEE (2017) [5](#)
 47. Xu, C., Zhang, J., Wang, M., Tian, G., Liu, Y.: Multilevel spatial-temporal feature aggregation for video object detection. *IEEE Transactions on Circuits and Systems for Video Technology* **32**(11), 7809–7820 (2022) [4](#)
 48. Xu, J., Cao, Y., Zhang, Z., Hu, H.: Spatial-temporal relation networks for multi-object tracking. In: Proceedings of the IEEE/CVF international conference on computer vision. pp. 3988–3998 (2019) [5](#)
 49. Ying, X., Wang, L., Wang, Y., Sheng, W., An, W., Guo, Y.: Deformable 3d convolution for video super-resolution. *IEEE Signal Processing Letters* **27**, 1500–1504 (2020) [8](#)
 50. Zhou, X., Koltun, V., Krähenbühl, P.: Tracking objects as points. *ECCV* (2020) [5](#), [10](#), [11](#), [12](#), [13](#), [14](#)
 51. Zhou, X., Wang, D., Krähenbühl, P.: Objects as points. In: arXiv preprint arXiv:1904.07850 (2019) [5](#), [10](#)
 52. Zhu, A.Z., Yuan, L., Chaney, K., Daniilidis, K.: Unsupervised event-based learning of optical flow, depth, and egomotion. In: Proceedings of the IEEE/CVF Conference on Computer Vision and Pattern Recognition. pp. 989–997 (2019) [4](#)
 53. Zihao Zhu, A., Yuan, L., Chaney, K., Daniilidis, K.: Unsupervised event-based optical flow using motion compensation. In: Proceedings of the European Conference on Computer Vision (ECCV) Workshops. pp. 0–0 (2018) [4](#)
 54. Zuiderveld, K.: Contrast limited adaptive histogram equalization. *Graphics gems* pp. 474–485 (1994) [13](#)

Supplementary Material

In the supplementary material, we provide additional video and some qualitative analysis to demonstrate why our TEDNet outperforms prior works by such significant amounts.

1 Supplementary Video

We provide a supplementary video, where the images from the main paper are captured, to demonstrate the problem of prior works and the result of our TEDNet. There are two cars remaining still for a very long time in the video, i.e., the left car remains still from 22.5 to 55.9 seconds and the right car remains still from 22.5 to 52.7 seconds. Tab. 6 shows the duration of missing bounding boxes of RED, DMANet, and HMNet in the video for the left and the right car, respectively. As mentioned in the main paper, the missing bounding boxes last 17.9 seconds in RED, 32.4 seconds in DMANet, and interweavingly in HMNet. In addition, the video from 37.6 to 38.6 seconds shows that the real occluded objects are tracked by RVT, CenterTrack, and PermaTrack, incurring many false positives. Instead, our TEDNet discards those real occluded objects achieving fewer false positives and higher mAP performance. The video is publicly available at <https://youtu.be/JCCZcmZ2oXU>.

2 Qualitative Analysis

We compare our TEDNet to the state-of-the-art event-based object detectors on *clean GT* to demonstrate why our TEDNet can improve the mAP significantly. The comparison can be divided into two parts, including fine-grained and category-level comparison. The confidence score is set to 0.4 for all of the models.

Table 6: The duration of missing bounding boxes in the supplementary video for the left and the right car, respectively.

Methods	Left Car	Right Car
RED	38.4 ~ 56.3 s	no missing bbox
DMANet	23.7 ~ 56.1 s	25.6 ~ 52.9 s
HMNet	30.9 ~ 31.0 s	no missing bbox
	34.1 ~ 34.8 s	
	36.2 ~ 36.8 s	
	46.1 ~ 46.4 s	
	48.2 ~ 49.0 s	
	49.2 ~ 49.7 s	
TEDNet	no missing bbox	no missing bbox

Table 7: Fine-grained comparison with the state-of-the-art event-based object detectors on **clean GT**. The number of objects shown in the table is the mantissa of scientific notation with base 10 and exponent 3. (GT: Total Ground Truth / DT: Total Detection / TP: True Positive / FP: False Positive / FN: False Negative)

Methods	RED	CenterTrack	PermaTrack	TEDNet
GT	1220	1220	1220	1220
DT	1466	1134	1307	<u>1218</u>
TP	829	836	<u>898</u>	930
FP(wrong id)*	29	24	34	<u>25</u>
FP(wrong bbox)†	608	<u>274</u>	376	263
FP	637	<u>298</u>	409	288
FN	362	359	<u>288</u>	264
Precision	56.6	<u>73.7</u>	68.7	76.3
Recall	68.0	68.6	<u>73.6</u>	76.3

The bold and the underline indicate the best and the second-best.

* Wrong id means the bounding box is correctly detected with the wrong category identity.

† Wrong bbox means the bounding box is incorrectly detected.

2.1 Fine-grained Comparison

We calculate the number of ground truths (GT), detections (DT), true positives (TP), false positives (FP), and false negatives (FN) with a predefined confidence score 0.4 as shown in Tab. 7. All of the numbers on our TEDNet are either the best or the second-best, where our TEDNet not only increases TPs and decreases FNs, but also decreases FPs significantly and decreases DTs, making it more robust than other models. In summary, our TEDNet achieves the highest precision and recall.

2.2 Category-level Comparison

We conduct category-level analysis to demonstrate the effectiveness of our TEDNet on still objects in Tab. 8 and moving objects in Tab. 9. The reason why the objects are split into still and moving objects in the category-level comparison is to prove our intuition of regarding still objects as pseudo-occlusion and exploiting tracking through occlusion to keep object permanence. For the still objects in Tab. 8, our TEDNet increases the TPs of all the categories by a significant amount, demonstrating the efficacy of tracking through pseudo-occlusion. For moving objects in Tab. 9, our TEDNet performs either the best or the second-best for every category, and it performs the best in total. In summary, our TEDNet can not only improve the number of TPs on still objects but also the number of TPs on moving objects, making it achieve state-of-the-art performance.

Table 8: Category-level comparison with the state-of-the-art event-based object detectors on **still objects** of **clean GT**. The number of detected objects (TP) shown in the table is the mantissa of scientific notation with base 10 and exponent 3.

Categories	GT	RED	CenterTrack	PermaTrack	TEDNet
pedestrian	27	11.9	12.3	<u>15</u>	18
two wheeler	7.9	3.6	4.6	<u>5.7</u>	6.0
car	90	50	70	<u>75</u>	79
truck	5.0	1.6	2.9	<u>3.1</u>	3.2
bus	4.3	1.5	<u>1.82</u>	1.7	1.83
traffic sign	19	3	8	<u>10</u>	11
traffic light	41	12	21	<u>25</u>	27
total	195	84	121	<u>134</u>	146

The bold and the underline indicate the best and the second-best.

Table 9: Category-level comparison with the state-of-the-art event-based object detectors on **moving objects** of **clean GT**. The number of detected objects (TP) shown in the table is the mantissa of scientific notation with base 10 and exponent 3.

Categories	GT	RED	CenterTrack	PermaTrack	TEDNet
pedestrian	286	<u>203</u>	178	200	213
two wheeler	41	26	28.9	30	<u>29.3</u>
car	480	405	397	<u>409</u>	410
truck	56	32	35	<u>40</u>	42
bus	19	<u>10</u>	9	8	12
traffic sign	78	40.6	<u>41.2</u>	40.9	44
traffic light	63	29	28	37	<u>36</u>
total	1025	746	716	<u>764</u>	785

The bold and the underline indicate the best and the second-best.